

ARTICLES

Analyzing powers of $p+d$ scattering below the deuteron breakup threshold

S. Shimizu,* K. Sagara, H. Nakamura, K. Maeda, T. Miwa, N. Nishimori, S. Ueno, T. Nakashima, and S. Morinobu

Department of Physics, Kyushu University, Fukuoka, 812 Japan

(Received 24 January 1995)

All the vector and tensor analyzing powers of the $p+d$ scattering have been measured at $E_p^{\text{lab}}=2.5$ MeV ($E_d^{\text{lab}}=5$ MeV), where a calculation of the three-nucleon scattering state with an improved treatment of Coulomb force has become available. Measurements have also been made at energies below and slightly above the deuteron breakup threshold at $E_p^{\text{lab}}=3.34$ MeV. The experimental data have small statistical errors ranging from ± 0.0004 to ± 0.0008 , and the uncertainties in the scale are less than 1%. The present data together with our previous data on the cross section are compared with several Faddeev calculations based on a separable-form nucleon-nucleon potential or on a realistic potential with Coulomb force being treated nearly correctly or approximately. Disagreements between the calculations and the experiment are found not only in the cross section and the vector analyzing powers A_y and iT_{11} but also in the tensor analyzing powers T_{21} and T_{22} .

PACS number(s): 25.10.+s, 24.70.+s, 25.45.De

I. INTRODUCTION

Recent progress in incorporating realistic nucleon-nucleon (NN) potentials [1,2] and three-nucleon ($3N$) forces [3] in the Faddeev calculation of the $3N$ scattering state has enabled the examination of various potential models in the light of $3N$ observables. For the examinations with the $p+d$ observables, however, a long-standing theoretical problem of the correct treatment of the Coulomb force in the $3N$ scattering state still remains unsolved. A breakthrough in this respect has been made by Berthold, Stadler, and Zankel [4] who succeeded in treating the Coulomb force nearly correctly for the $p+d$ scattering state at $E_p=2.5$ MeV, slightly below the deuteron breakup threshold at 3.34 MeV. Although their calculation is based on a simple separable-form NN potential, it is of great use in discriminating the Coulomb effects from the nuclear contribution in the cross section and the analyzing powers of the $p+d$ scattering. In these circumstances, high-precision experimental data on the $p+d$ scattering at 2.5 MeV could provide valuable information on the NN interactions through the detailed comparison with the Faddeev calculations.

For the $\vec{n}+d$ and the $\vec{p}+d$ scatterings below 20 MeV, a large discrepancy of about 25% between the experiment and the calculation is well known to exist in A_y [5]. Improvements of the calculation have been examined by modifying the vector part of the NN potentials [6,7] or by introducing $3N$ forces [3,8], although no satisfactory explanation has been obtained yet. Moreover, our previous work below 18 MeV [9] has revealed a discrepancy of the same order of magnitude in the $p+d$ differential cross section, which may indicate a necessity of some improvement in the scalar part of the NN potential also. Although a similar situation may be

expected for the tensor part of the NN potential, no detailed comparison has been available between the experiment and the calculation. For a consistent examination of all the parts of the NN potential, it is very interesting to measure the tensor analyzing powers with enough precision to see the possible deviations of experimental results from the recent calculations.

In this paper, we report on the precise measurements of the vector analyzing power A_y of the $\vec{p}+d$ scattering at $E_p=2, 2.5, 3,$ and 4 MeV and of the vector and tensor analyzing powers $iT_{11}, T_{20}, T_{21},$ and T_{22} of the $\vec{d}+p$ scattering at $E_d=5$ and 6 MeV which correspond to the c.m. energies for $E_p=2.5$ and 3 MeV, respectively, in the case of proton incidence. We have already reported the differential cross section of the $p+d$ scattering in this energy range [9]. All these data are compared with the nearly correct Coulomb calculation [4] as well as with the calculations [10] based on a realistic NN potential with the Coulomb force being treated in a conventional approximation [11].

II. EXPERIMENT ON ${}^2\text{H}(\vec{p},p)$ SCATTERING

The analyzing power A_y of the ${}^2\text{H}(\vec{p},p)$ scattering at 2–4 MeV was measured in a way similar to that adopted in our previous experiment on A_y at 5–18 MeV [9].

A. Experimental setup

A polarized proton beam from the Kyushu University tandem accelerator was used to bombard the target deuterium gas of up to 0.27 atm in a cylindrical cell placed in vacuum in a scattering chamber (Fig. 1). The structure of the cell has been described in Ref. [9]. To reduce the angular spread of low-energy particles due to the multiple scattering in the target cell windows, we adopted thin and low-atomic-number foils, i.e., 2- μm -thick and 4- μm -thick aluminum foils for the

*Present address: Department of Mechanical Engineering, Yamaguchi University, Ube, 755 Japan.

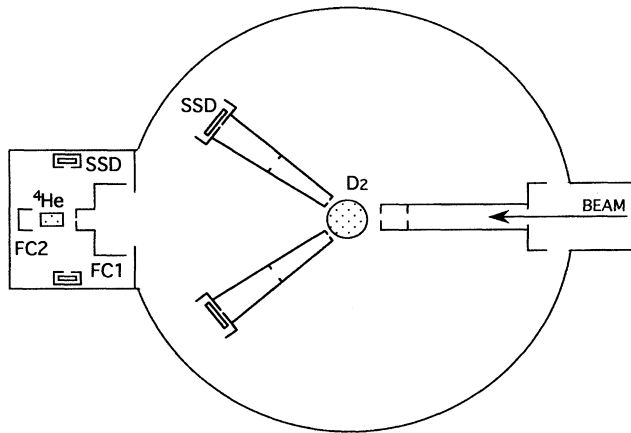


FIG. 1. Plane view of the setup for the ${}^2\text{H}(\vec{p}, p)$ experiment in a 1-m-diam vacuum chamber. A proton beam polarimeter using the $\vec{p}+{}^4\text{He}$ scattering was placed at the beam dump. The Faraday cup is divided into two parts to collimate the beam incident on the polarimeter (FC1) and to measure the current passed through the polarimeter (FC2).

beam entrance and the exit windows, respectively, and 1.5- μm -thick Mylar foils for the side windows.

Two particle counters were placed in the scattering chamber symmetrically on the left and the right sides of the beam axis to detect the scattered protons and the recoil deuterons from the $p+d$ scattering. Each of the counters consisted of a Si detector and a double-slit system consisting of a 2-mm-wide vertical slit and a slit of a 6-mm-wide and 15-mm-high aperture, located at 5 cm and 40 cm apart from the target center, respectively.

The geometrical angular spread [full width at half maximum (FWHM)] defined by the slit system was $\pm 0.49^\circ$. The angular spread of the particles due to the multiple scattering in the side windows of the target cell was estimated [12] to range from $\pm 0.14^\circ$ for 3.8 MeV protons to $\pm 0.96^\circ$ for 0.7 MeV deuterons, and the angular spread of the proton beam caused by the entrance window was calculated to be from $\pm 0.37^\circ$ at 4 MeV to $\pm 0.74^\circ$ at 2 MeV. The angular spreads of the proton beam and the scattered particles caused by the target gas were estimated to be several times smaller than the spreads described above. The total angular spread was small enough to enable the measurement of slowly varying angular distribution of A_y without attenuation. The direction of the beam axis was determined to $\pm 0.1^\circ$ as in Ref. [9], and the counter angles were set within $\pm 0.1^\circ$.

The polarization of the beam was measured throughout the experiment by a $\vec{p}+{}^4\text{He}$ polarimeter placed at the downstream end of the scattering chamber (see Fig. 1). A part of the beam passing through an aperture of 4 mm in diameter at the bottom of the first Faraday cup was incident on the polarimeter target of 0.5 atm ${}^4\text{He}$ gas, and was finally stopped in the second Faraday cup. The beam charge in the second Faraday cup was used to determine the beam polarization, and the total beam charge was used to deduce the $\vec{p}+d$ A_y . The ${}^4\text{He}$ target cell of the polarimeter had a beam entrance window of a 4- μm -thick aluminum foil and two side windows of a 1.5- μm -thick Mylar foil. Protons scattered by

the ${}^4\text{He}$ target were detected by two counters placed symmetrically on the left and the right sides of the beam axis. The counters were set at the angle where the $\vec{p}+{}^4\text{He}$ A_y takes the maximum value.

The present polarimeter measures the polarization of a part of the incident beam. It was confirmed from the calculation that the possible variation of the beam polarization across the beam profile at the deuterium target was completely smeared out at the polarimeter target by the multiple scattering of the beam at the entrance and the exit windows of the deuterium target cell. Hence, the polarization measured by the polarimeter was considered to a good accuracy to be equal to the average polarization of the incident beam. Moreover, since the same setup was used both in the $\vec{p}+d$ experiment and in the polarimeter calibration experiment, the spatial variation of the beam polarization, if present, was expected to cause no influence on the measured $\vec{p}+d$ A_y .

B. Analyzing power of the proton beam polarimeter

To evaluate A_y of the proton beam polarimeter, experimental asymmetries ($p_y A_y$) in the $\vec{p}+{}^4\text{He}$ scattering were measured simultaneously by the polarimeter and by the setup for the $\vec{p}+d$ experiment in the scattering chamber (upstream setup) with helium gas in place of deuterium gas. The beam energy was set to be 2.00, 2.50, 3.00, and 4.00 MeV at the center of the upstream target.

First, by using the upstream setup as a monitor for the beam polarization (p_y), the relative angular distribution of the polarimeter A_y was measured to find the angle of the maximum A_y . Next, the polarimeter counters were set at the angle of the maximum A_y to monitor the beam polarization, and the relative angular distribution of the $\vec{p}+{}^4\text{He}$ A_y around its maximum was measured by the upstream setup within a statistical accuracy of 0.3%. The measured angular distribution was found to be well reproduced by any of the three sets of the phase shifts which have been reported independently for the $\vec{p}+{}^4\text{He}$ scattering in the energy ranges of $0 \leq E_p \leq 5$ MeV [13], $0 \leq E_p \leq 18$ MeV [14], and $1.1 \leq E_p \leq 2.15$ MeV [15]. The maximum A_y values in the angular distribution calculated from the three sets of the phase shifts agreed well with each other, especially near 2 MeV where the $\vec{p}+{}^4\text{He}$ A_y takes the theoretical limit of $A_y = 1$ [16]. The maximum difference among the calculated values was 0.6% at 3 MeV. Finally, by normalizing the measured relative A_y to the values calculated from the phase shifts in Ref. [13], we determined the polarimeter A_y , which was higher than 0.901 for the beam energies of 2–4 MeV. From the uncertainties in the phase shifts adopted and the statistical errors in the measurement above, the uncertainty in the polarimeter A_y was estimated to be within 1% at 3 MeV and within 0.7% at the other energies.

C. Experimental procedure

Both the scattered protons and the recoil deuterons from the ${}^2\text{H}(\vec{p}, p)$ scattering were measured in the laboratory angular range of 16° – 52° at intervals of 2° . The c.m. angular ranges of 23.9° – 75.2° and 148° – 76° were covered by the proton and the deuteron measurements, respectively. The

proton and the deuteron counts were obtained by integrating the energy spectra around the respective peaks in the same manner as described in Ref. [9]. The integration range for a peak was typically the full width at 1/20 maximum. By changing the integration range, the background contribution to A_y was found to be ± 0.0001 or less, and was neglected in the final results.

The beam intensity of typically 150 nA and the target gas pressure of up to 0.27 atm were controlled so as to keep the counting rates in the counters below 6×10^3 counts/sec, which caused a dead time of 2.5% in the counting system. The dead time correction to A_y was negligibly small. More than 4×10^6 counts of the protons and the deuterons were accumulated at every angle.

The direction of the beam polarization was flipped upward and downward every 10 sec by reversing the magnetic field strength in the spin filter of the ion source. The beam polarization was measured by the beam polarimeter within a statistical accuracy of 0.3% in every experimental run of 15–30 min measurement, and was typically 0.79 and 0.55 for the spin-up and spin-down beams, respectively.

At each angle, two $\vec{p}+d$ A_y values were obtained independently from the measurements by the left and the right counters as in Ref. [9]. The values, after being confirmed to agree with each other within statistical fluctuations, were averaged to give the final A_y .

III. EXPERIMENT ON $H(\vec{d},d)$ SCATTERING

The vector and tensor analyzing powers of the $H(\vec{d},d)$ scattering at 5 and 6 MeV were measured using a polarized deuteron beam from the Kyushu University tandem accelerator.

A. Experimental setup

Different setups were used for the measurements in the three angular ranges of $7^\circ \leq \theta_{\text{lab}} \leq 16^\circ$, $16^\circ \leq \theta_{\text{lab}} \leq 27^\circ$, and $27^\circ \leq \theta_{\text{lab}} \leq 45^\circ$. The measurements in the backward and middle angular ranges were made with the same target cell as used in the ${}^2\text{H}(\vec{p},p)$ experiment. The forward-angle measurement was carried out with a specially designed target cell having a horizontally wide exit window (4- μm -thick aluminum foil) through which both the beam and the scattered particles came out. In all the angular ranges, two counters were placed symmetrically to the left and the right of the beam axis. Since the recoil deuterons are emitted within $\theta_{\text{lab}} \leq 30^\circ$, counter telescopes each consisting of a 30- μm -thick Si ΔE detector and a 450- μm -thick Si E detector were used to separate the deuterons from the scattered protons in the forward and middle angular ranges. In the backward angular range, only the E detectors were used to detect the protons. The counters were equipped with double slits at the same positions as described in Sec. II A. The widths of the front vertical slits were 3 mm and the apertures of the rear slits were 4 mm in width and 10 mm in height for the middle angular range. The front-slit widths were reduced to 2 mm in the forward angular range, considering high counting rates in the counters. In the backward angular range, the rear slit apertures 1.5 times as large both in width and in height

were used to approximately equate the c.m. solid angles for the protons to those for the deuterons in the middle angular range.

The deuteron beam polarization was measured throughout the experiment with a polarimeter [17] placed downstream of the scattering chamber. The polarimeter used $T_{20}(0^\circ)$, $T_{21}(150^\circ)$, and $iT_{11}(127.5^\circ)$ of the ${}^3\text{He}(\vec{d},p)$ reaction. For the present low-energy experiment, the window foils of the polarimeter target cell were 2.2- μm -thick Havar foils.

B. Analyzing powers of the deuteron polarimeter

The absolute value of $T_{20}(0^\circ)$ of the ${}^3\text{He}(\vec{d},p)$ reaction takes the maximum value at $E_d = 5.6$ MeV. The polarimeter analyzing power $T_{20}(0^\circ)$ at this energy was determined using the ${}^{16}\text{O}(\vec{d},\alpha_1){}^{14}\text{N}(0^+)$ reaction whose tensor analyzing powers are theoretically known [18] as $A_{yy} = -2$, $A_{xx} = A_{zz} (= T_{20}/\sqrt{2}) = 1$. To cope with the small cross section of the isospin forbidden ${}^{16}\text{O}(d,\alpha_1)$ reaction, the target was made thick as long as the multiple scattering in the target and the target cell windows did not cause harmful backgrounds in the α spectrum. The oxygen target gas of 0.2 atm was sealed in a cylindrical cell of 22 mm in diameter having 4- μm -thick aluminum foils for the beam entrance and the exit windows and 1.5- μm -thick Mylar foils for the side windows. The left and right counters had 50- μm -thick Si detectors to separate the α particles from the deuterons. The (d,α_1) reaction cross section was about 0.7 mb/sr at $E_d = 6.1$ MeV and $\theta_{\text{lab}} = 35^\circ$, and about 2×10^6 counts of α particles from the reaction were accumulated in a day. The linearly interpolated background for the α_1 peak was about 0.3%. From the simultaneous measurements of the beam polarization t_{20} using the ${}^{16}\text{O}(\vec{d},\alpha_1)$ reaction and of the polarimeter asymmetry $t_{20}T_{20}$, the polarimeter T_{20} at $E_d = 5.6$ MeV was determined. After the corrections for the depolarization effects in the ion source described below, the value was -1.255 with an overall accuracy of $\pm 0.5\%$.

The energy dependence of the polarimeter $T_{20}(0^\circ)$ at $E_d = 4\text{--}6$ MeV was determined by referring to the reported values of $T_{20}(0^\circ)$ for the ${}^3\text{He}(\vec{d},p)$ reaction by Gruebler *et al.* [19]. To measure $T_{20}(0^\circ)$ of the ${}^3\text{He}(\vec{d},p)$ reaction, a setup consisting of a ${}^3\text{He}$ gas target, a Faraday cup for the \vec{d} beam, and a counter telescope for protons at 0° were installed in the scattering chamber. The counter telescope had the same angular acceptance as that in Ref. [19]. The asymmetry $t_{20}T_{20}(0^\circ)$ in the setup and that in the polarimeter were measured alternately for the same beam polarization t_{20} in the energy range of 4–6 MeV. From the ratio of the asymmetries and the reported T_{20} values, the polarimeter $T_{20}(0^\circ)$ was evaluated within an accuracy of $\pm 0.3\%$ not including the uncertainty of $\pm 1\%$ in the reference values. The polarimeter $T_{20}(0^\circ)$ at 5.6 MeV thus evaluated was 0.3% larger than the value determined from the ${}^{16}\text{O}(\vec{d},\alpha_1)$ reaction. Hence, all the evaluated values were reduced by 0.3%.

The polarimeter analyzing power $T_{21}(150^\circ)$ at 4–6 MeV was determined from the ratio of the asymmetries in the polarimeter, $t_{21}T_{21}(150^\circ)/t_{20}T_{20}(0^\circ)$, and the polarimeter $T_{20}(0^\circ)$ described above. The ratio of the beam polarizations

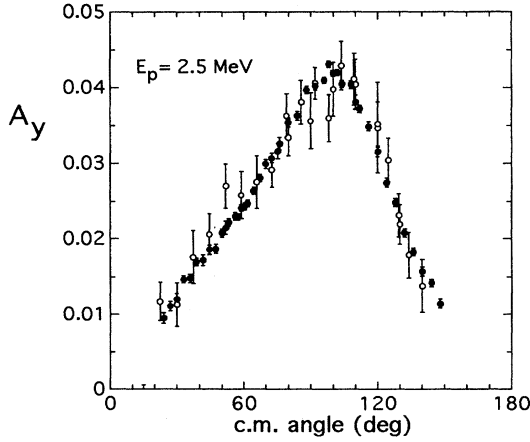


FIG. 2. Present data (solid circles) and previous data [19] (open circles) for A_y of the ${}^2\text{H}(\vec{p}, p)$ scattering at $E_p = 2.5$ MeV.

t_{21}/t_{20} depends sharply on the angle β between the beam polarization axis and the beam axis. First, the electric field strength of the spin precessor in the ion source was calibrated in β by observing two $t_{20}=0$ points at $\beta=54.7^\circ$ and 125.3° . Next the asymmetry ratio was measured at the settings of $\beta = 20^\circ, 45^\circ, 70^\circ$, and 90° . From these data and the β dependence of the t_{21}/t_{20} ratio, the ratio of $T_{21}(150^\circ)/T_{20}(0^\circ)$ was determined within a statistical accuracy of $\pm 0.4\%$. In this procedure, the reproducibility of β was found to be within $\pm 0.3^\circ$.

The ratio of $iT_{11}(127.5^\circ)/T_{20}(0^\circ)$ at 4–6 MeV was determined within a statistical error of $\pm 0.3\%$ from the ratio of the polarimeter asymmetries, $it_{11}iT_{11}(127.5^\circ)/t_{20}T_{20}(0^\circ)$ measured at $\beta=90^\circ$, using the equality relation between the vector and tensor polarization in the Lamb-shift polarized-ion source.

Both in the polarimeter calibration and in the $p+\vec{d}$ experiment, the ion source setting for the deuteron magnetic substate was cyclically changed over $m=1, 0$ and -1 at intervals of 10, 20, and 10 sec, respectively. The polarizations in the substates were slightly different to each other. The difference caused in the spin-filter section in the ion source was estimated from the resonance curve of the beam intensity against the magnetic field in the spin filter. The difference caused by the depolarization in the subsequent charge-transfer section was evaluated according to the formulas in Ref. [20]. The corrections to the beam polarization due to the former and the latter effects were within $\pm 0.3\%$ and $\pm 2\%$, respectively. The corrections to the analyzing powers were less than $\pm 0.2\%$, since the asymmetries were measured simultaneously by the polarimeter and by the upstream setup for the same beam polarization.

The total uncertainties in the polarimeter $T_{20}(0^\circ)$, $T_{21}(150^\circ)$, and $iT_{11}(127.5^\circ)$ determined in the energy range of 4–6 MeV were estimated to be within 1% which mainly came from the errors of the reference values [19].

C. Experimental procedure

The angular distribution of the $\text{H}(\vec{d}, d)$ scattering was measured by detecting the scattered deuterons at $\theta_{\text{lab}}=7^\circ-$

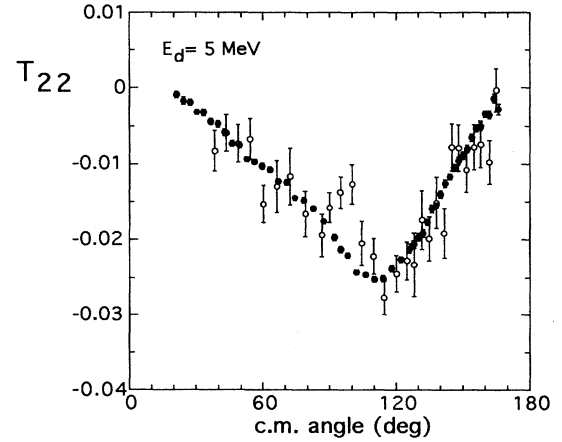


FIG. 3. Present data (solid circles) and previous data [19] (open circles) for T_{22} of the $\text{H}(\vec{d}, d)$ scattering at $E_d = 5$ MeV.

27° ($\theta_{\text{c.m.}}=21^\circ-92^\circ$) and the recoil protons at $\theta_{\text{lab}}=7^\circ-45^\circ$ ($\theta_{\text{c.m.}}=166^\circ-90^\circ$). To measure the whole analyzing powers iT_{11} , T_{20} , T_{21} , and T_{22} of the $\text{H}(\vec{d}, d)$ scattering, the following three spin directions were chosen: (a) $\beta=0^\circ$, (b) $\beta=45^\circ$, both with the beam polarization axis in the reaction plane, and (c) $\beta=90^\circ$ with the beam polarization axis along the normal (y) to the reaction plane. The setting of the azimuthal angle ϕ between the reaction plane and the plane normal to the beam polarization axis was checked by simultaneously measuring the beam polarizations p_x and $p_y (=2it_{11}/\sqrt{3})$ which vary as $\cos\phi$ and $\sin\phi$, respectively. The setting error in ϕ was within $\pm 1^\circ$, which caused negligibly small contribution to the final results. The analyzing powers T_{20} , T_{21} , and iT_{11} were measured with the spin directions (a), (b), and (c), respectively, and T_{22} was evaluated from the measurements with the directions (a) and (c).

Using the beam polarimeter, the tensor and the vector polarization of the beam was determined within a statistical accuracy of 0.5% in each experimental run. The beam polarization observed was typically 0.70.

More than 2×10^6 counts of the scattered deuterons and the recoil protons were accumulated at every angle adopted. The beam intensity and the target gas pressure, which were less than 300 nA and 0.27 atm, respectively, were so controlled as to keep the counting rate below 6×10^3 counts/sec, which caused a dead time of 2.5% in the counting system. The dead time corrections were less than 0.0005 for T_{20} and T_{22} , and were negligibly small for iT_{11} and T_{21} .

IV. EXPERIMENTAL RESULTS

High-precision data on $A_y(\theta)$ of the $\vec{p}+d$ scattering were obtained in the angular range of $\theta_{\text{c.m.}}=23.9^\circ-148^\circ$ at $E_p^{\text{lab}}=2.00, 2.50, 3.00$, and 4.00 MeV. The typical statistical error in A_y was ± 0.0005 , including the statistical error in the beam polarization measurement. The error in the scale of A_y was estimated to be within $\pm 1\%$ at 3 MeV, and within $\pm 0.7\%$ at the other energies.

Precise data on the analyzing powers of $iT_{11}(\theta)$, $T_{20}(\theta)$, $T_{21}(\theta)$, and $T_{22}(\theta)$ of the $p+\vec{d}$ scattering were also

taken in the angular range of $\theta_{\text{c.m.}} = 21^\circ - 166^\circ$ at $E_d^{\text{lab}} = 5.00$ and 6.00 MeV, i.e., at the same c.m. energies as $E_p^{\text{lab}} = 2.50$ and 3.00 MeV, respectively. The typical statistical errors ranged from ± 0.0004 for iT_{11} to ± 0.0008 for T_{20} . The scaling errors of the analyzing powers were estimated to be within $\pm 1\%$.

The present data at $E_p = 2.5$ MeV and at $E_d = 5$ MeV have much higher statistical accuracy than previous ones [21] though both data agree with each other, as typically seen in Figs. 2 and 3. The present data are also in good agreement with the similarly accurate data taken at $E_p = 3$ MeV and at $E_d = 6$ MeV [22].

The high statistical accuracy of the present data was due mainly to the use of high-intensity polarized beams together with high-pressure gas targets. The latter was realized by adopting high-tensile, thin, and low-atomic-number foils for the target cell windows.

The accuracies in the scales of the analyzing powers have also been improved by the careful calibrations of the beam polarimeters with high statistical accuracies. The scaling error of A_y mainly came from the uncertainty in the $p+{}^4\text{He}$ phase shifts adopted [13], and those of $iT_{11}(\theta)$, $T_{20}(\theta)$, $T_{21}(\theta)$, and T_{22} largely from the reported error in the energy dependence of $T_{20}(0^\circ)$ for the ${}^3\text{He}(\vec{d},p)$ reaction [19].

V. COMPARISON WITH FADDEEV CALCULATIONS

The present experimental data on the $p+d$ analyzing powers and our previous data on the $p+d$ differential cross section in the same energy range [9] were compared with six kinds of Faddeev calculations, which are hereafter denoted by PEST.exC, PEST.apC, PEST.noC, Paris.apC, Paris.noC, and modLS.apC, according to the NN potentials used and the Coulomb force treatments employed. The first three calculations were performed by Berthold, Stadler, and Zankel [4] using the PEST16 potential which is a rank-1 separable-form potential obtained from the Paris NN potential. In PEST.exC, the Coulomb force was treated nearly correctly by replacing the two-body Coulomb t matrix in the three-body formalism by the Coulomb potential [4]. In PEST.apC, the Coulomb force was treated approximately in the manner proposed by Doleschall *et al.* [11], who replaced the $p+d$ scattering amplitude by the sum of the $p+d$ Rutherford amplitude and the $n-d$ amplitude (calculated in the three-body formalism) having the Coulomb phases of $p+d$ two-body scattering. The Coulomb force was switched off in PEST.noC. The remaining three calculations were made using the code by Takemiya [10]. The original form of the Paris potential was used in Paris.apC and Paris.noC. The Coulomb force was treated approximately in the former and switched off in the latter. In modLS.apC, a NN potential obtained by enhancing the short-range (~ 1.5 fm) part of the LS force in the Paris potential [7] was adopted and the Coulomb force was included approximately.

In (a) of Figs. 4–9, the experimental results (solid circles) at $E_p = 2.5$ MeV ($E_d = 5$ MeV) are compared with PEST.exC (solid curves), PEST.apC (dashed ones), and PEST.noC (dotted ones). In (b) of Figs. 4–9, modLS.apC (solid curves), Paris.apC (dashed ones), and Paris.noC (dotted ones), are shown together with the same experimental data. In (c) of Figs. 4–9 the experimental results at the other energies are

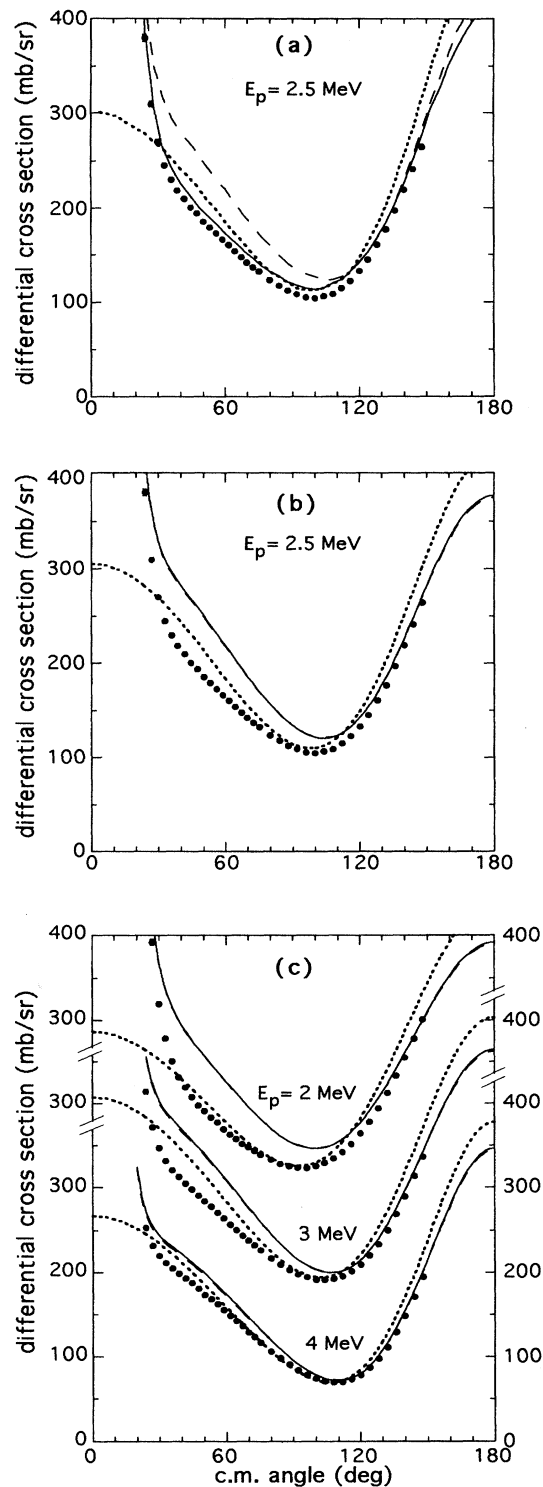


FIG. 4. Differential cross section of the ${}^2\text{H}(p,p)$ scattering at $E_p = 2-4$ MeV [5]. The experimental errors are within the sizes of the data points. The curves are the results of the Faddeev calculations described in the text. The curves in (a) represent PEST.exC (solid line), PEST.apC (dashed line), and PEST.noC (dotted line) [4]. The curves in (b) and (c) are modLS.apC (solid line), Paris.apC (dashed line), and Paris.noC (dotted line) [6]. Note that the solid and dashed curves in (b) and (c) almost coincide.

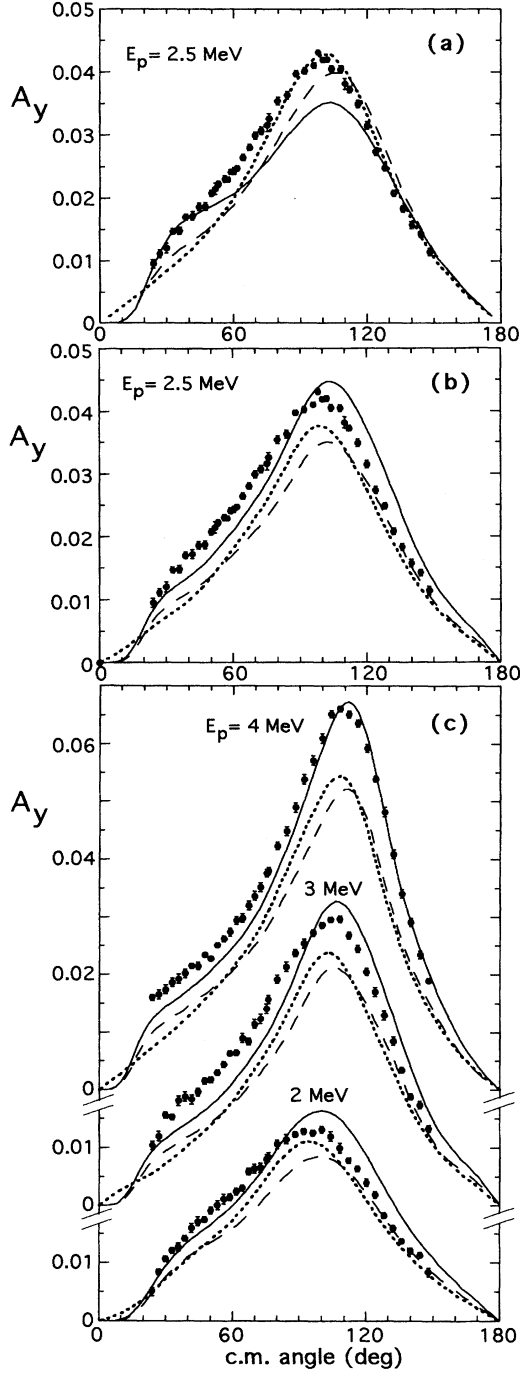


FIG. 5. A_y of ${}^2\text{H}(\vec{p}, p)$ scattering at $E_p = 2.5$ MeV. The curves in (a) represent PEST.exC (solid line), PEST.apC (dashed line), and PEST.noC (dotted line) [4]. The curves in (b) and (c) are modLS.apC (solid line), Paris.apC (dashed line), and Paris.noC (dotted line) [6].

compared with modLS.apC (solid ones), Paris.apC (dashed ones), and Paris.noC (dotted ones). One can see the comparison between PEST.exC and the precise experiment at $E_p = 3$ MeV ($E_d = 6$ MeV) in Ref. [22].

If the PEST16 potential is equivalent to the original Paris potential, PEST.apC and PEST.noC [dashed and dotted

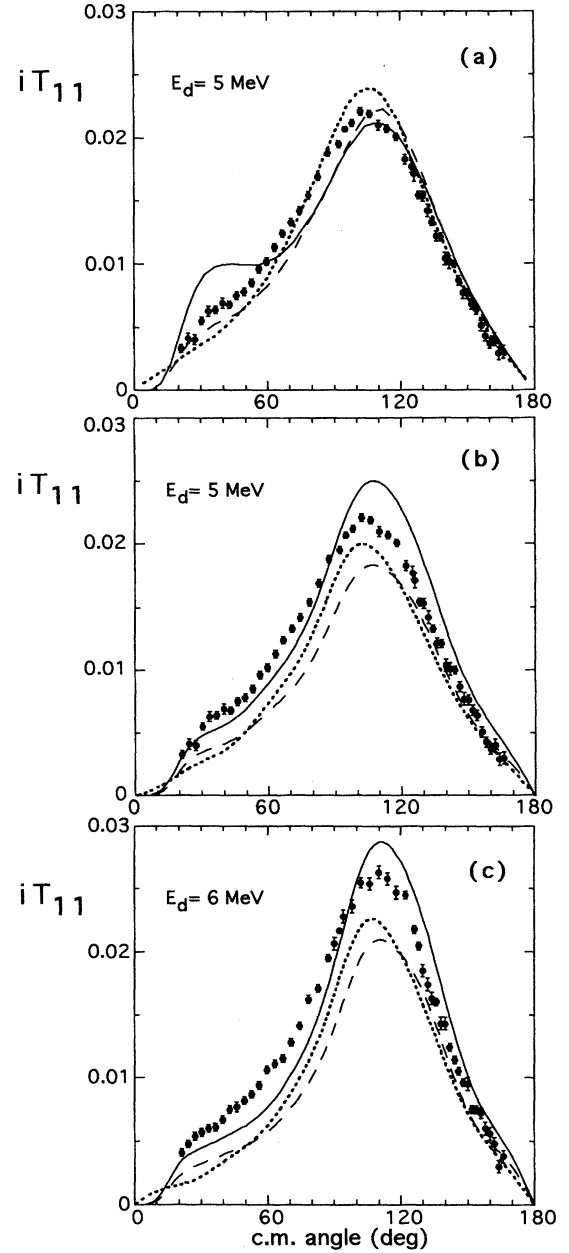


FIG. 6. The iT_{11} of the $\text{H}(\vec{d}, d)$ scattering at $E_d = 5$ and 6 MeV. The curves in (a) represent PEST.exC (solid line), PEST.apC (dashed line), and PEST.noC (dotted line) [4]. The curves in (b) and (c) are modLS.apC (solid line), Paris.apC (dashed line), and Paris.noC (dotted line) [6]. The solid and dashed curves in (b) and (c) almost coincide.

curves in (a)] should coincide with Paris.apC and Paris.noC [dashed and dotted ones in (b)], respectively. The two potentials give almost the same results for the cross section (Fig. 4), while different results are seen in the analyzing powers (Figs. 5–9).

It is highly desired to compare the experiment with a calculation based on the Paris potential together with the exact treatment of the Coulomb force (i.e., Paris.exC). Although Paris.exC has not been carried out yet, the following rela-

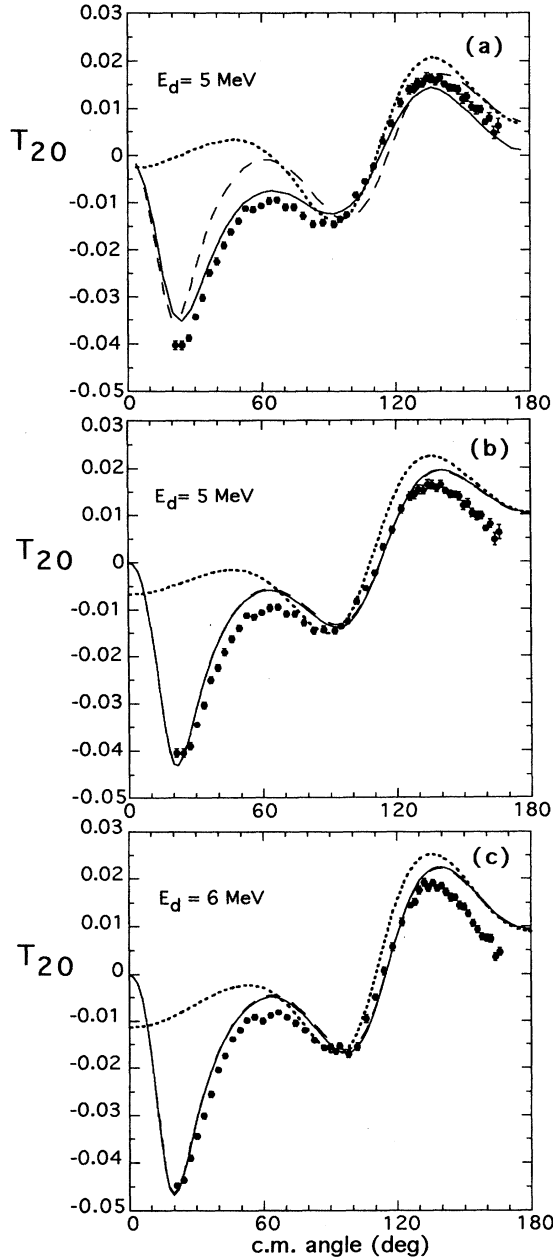


FIG. 7. T_{20} of the $H(\vec{d},d)$ scattering at $E_d = 5$ and 6 MeV. The curves are the same as those in Fig. 6.

tions may give a semi quantitative measure for the calculation:

$$\text{Paris.exC} \approx \text{Paris.noC} + (\text{PEST.exC} - \text{PEST.noC}), \quad (1)$$

$$\text{Paris.exC} \approx \text{Paris.apC} + (\text{PEST.exC} - \text{PEST.apC}). \quad (2)$$

A. Differential cross section

Figure 4(a) shows that the differential cross section of the $p+d$ scattering at $E_p = 2.5$ MeV is fairly well reproduced by PEST.exC, though the calculation is slightly above the experiment in the whole angular range. It is seen from the

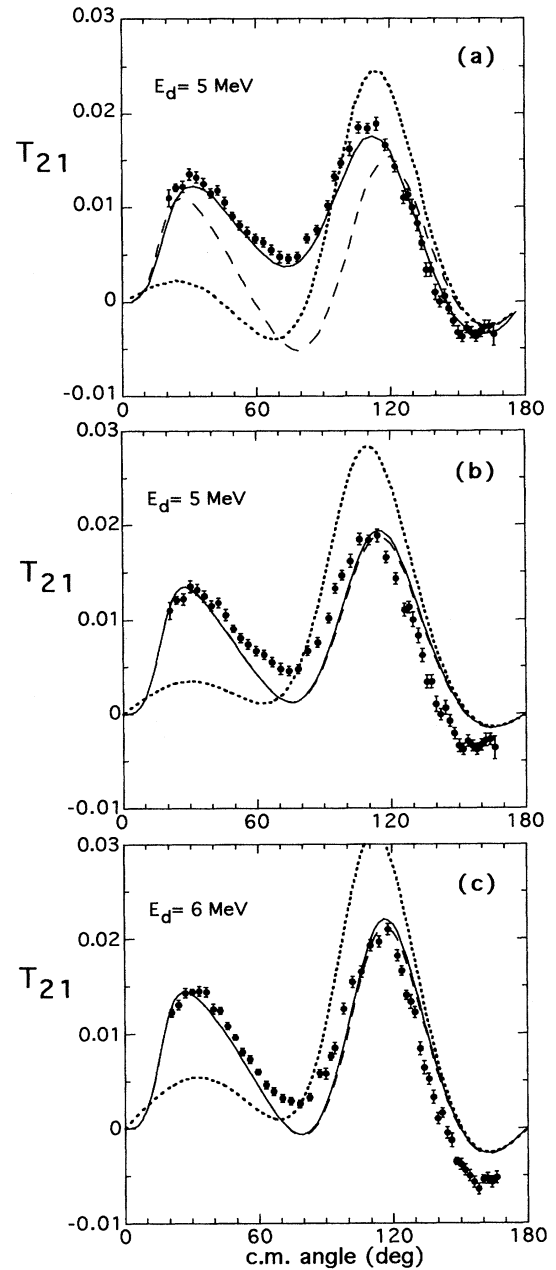


FIG. 8. T_{21} of the $H(\vec{d},d)$ scattering at $E_d = 5$ and 6 MeV. The curves are the same as those in Fig. 6.

comparison of PEST.exC with PEST.noC that the cross section at $\theta_{c.m.} < 30^\circ$ is dominated by the Rutherford scattering while the Coulomb effect is very small at $80^\circ < \theta_{c.m.} < 115^\circ$. At $115^\circ < \theta_{c.m.} < 150^\circ$, PEST.apC almost coincides with PEST.exC. From the relations (1) and (2), Paris.exC is expected to be almost equal to Paris.noC at $80^\circ < \theta_{c.m.} < 115^\circ$ and to Paris.apC at $115^\circ < \theta_{c.m.} < 150^\circ$. As seen in Fig. 4(b), the experimental results differ from Paris.noC at $80^\circ < \theta_{c.m.} < 115^\circ$ and from Paris.apC at $115^\circ < \theta_{c.m.} < 150^\circ$. The difference is 5–10 %, which is not very small compared with the well-known difference of 20–30 % in A_y . A similar difference may be expected between

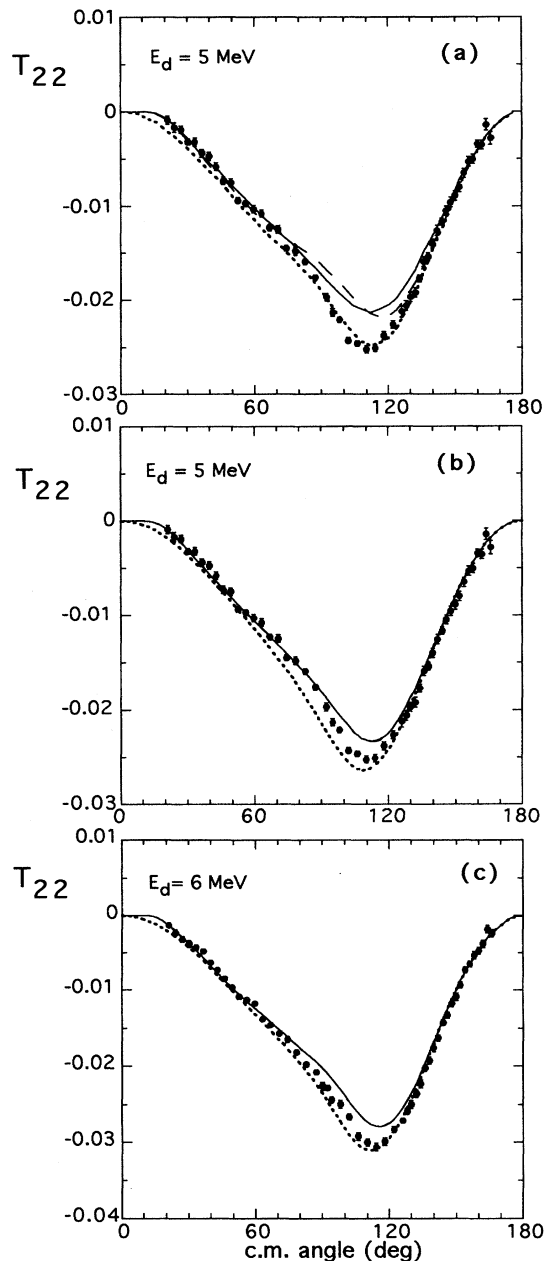


FIG. 9. T_{22} of the $H(\vec{d},d)$ scattering at $E_d = 5$ and 6 MeV. The curves are the same as those in Fig. 6.

the experiment and Paris.exC. This indicates that some improvement may also be necessary in the scalar part of the NN potential, although the true difference should be confirmed by the actual Paris.exC calculation. Figure 4(b) shows that Paris.apC and modLS.apC give almost the same cross section, implying that the modification in the LS potential has very small effect on the prediction of the cross section.

Differential cross sections at $E_p = 2, 3$ and 4 MeV are shown in Fig. 4(c). Paris.noC and Paris.apC around 115° may be expected to be close to Paris.exC, as in the case at 2.5 MeV. As the energy increases from 2 to 4 MeV, the differences between the experiment and the two calculations around 115° become small, and Paris.apC comes close to the

experiment in the whole angular range. Paris.exC may also be expected to become close to the experiment at 4 MeV. It has been reported [9], however, that Paris.apC falls below the experiment at above 12 MeV and that the energy-dependent difference between the experiment and Paris.apC may not fully be attributed to the approximation for the Coulomb force.

B. Vector analyzing powers A_y and iT_{11}

As seen in Fig. 5(a), the Coulomb force enhances the A_y value at around 30° and PEST.exC agrees well with the experiment. The Coulomb effect is large around the A_y maximum near 100° , where the effect on the cross section is very small. Around the A_y maximum, a large discrepancy is seen between PEST.exC and the experiment. An even larger discrepancy is expected between the possible Paris.exC and the experiment from relations (1) and (2), because the Paris.noC (Paris.apC) in Fig. 5(b) predicts lower value for the A_y maximum than PEST.noC (PEST.apC) in Fig. 5(a). The existence of the discrepancy around the A_y maximum has been well known for $N+d$ scattering below about $E_N = 20$ MeV [5]. The origin of the discrepancy has been searched for by assuming charge independence breaking in nuclear interactions [6], by modifying the LS part of the NN potential [7], or by introducing a three-nucleon force [3,8]. As seen in Fig. 5(b), the modification of the LS potential (modLS.apC) increases the A_y value in the whole angular range.

Figure 5(c) shows A_y at $E_p = 2, 3$, and 4 MeV. As the energy increases from 2 to 4 MeV, modLS.apC becomes close to the experiment in the whole angular range. It has been pointed out in our previous paper [9] that the A_y maximum predicted by modLS.apC agrees with the experiment at $E_p = 5-10$ MeV. However, it becomes smaller than the experiment at above 12 MeV if the same modified- LS potential is used. Some other refinement on the vector part of NN potentials is necessary.

The bump of iT_{11} at around 30° in PEST.exC is too high as seen in Fig. 6(a). However, since Paris.apC (Paris.noC) in Fig. 6(b) is fairly below PEST.apC (PEST.noC) in Fig. 6(a) around 30° , Paris.exC is expected from relations (1) and (2) to come close to the experiment. Around the iT_{11} maximum near 105° , however, a large discrepancy between the experiment and Paris.exC is expected because Paris.exC would be a little below Paris.apC [relation (2)]. The modification in the LS potential increases the iT_{11} value in the whole angular range as in the case for A_y . However, the difference between modLS.apC and the experiment for the iT_{11} maximum is slightly larger than that for the A_y maximum. This might indicate that somewhat different features of the nuclear interaction can be detected in the two vector analyzing powers A_y and iT_{11} .

C. Tensor analyzing powers T_{20} , T_{21} , and T_{22}

The modification in the LS potential has essentially no effects on all the tensor analyzing powers, as seen in (b) and (c) of Figs. 7–9 where Paris.apC and modLS.apC almost coincide with each other in the whole angular range.

PEST.exC and PEST.apC give nearly the same results for the deep dip of T_{20} at around 20° [Fig. 7(a)], and the experimental depth is reproduced well by the Paris.apC [Figs. 7(b)

and 7(c)]. This may suggest that the dip will be well reproduced by Paris.exC. At backward angles of $\theta_{c.m.} > 130^\circ$, Paris.exC is also expected to give correct T_{20} values because the difference between the experiment and Paris.apC (Paris.noC) is roughly equal to that between PEST.exC and PEST.apC (PEST.noC).

Coulomb effect is large in T_{21} as seen in Fig. 8. The difference between the experiment and Paris.apC at $\theta_{c.m.} > 130^\circ$, shown in Figs. 8(b) and 8(c), is expected to be reduced if the Coulomb force is treated correctly. Around the T_{21} maximum at 110° , however, Paris.exC may overestimate the experimental peak height at $E_d = 5$ and 6 MeV.

PEST.exC and PEST.apC give nearly the same results for T_{22} in the whole angular range as seen in Fig. 9(a). It is considered, therefore, that the difference in T_{22} around 110° between the experiment and Paris.apC [Figs. 9(b) and 9(c)], cannot fully be attributed to the approximate treatment of the Coulomb force.

It is very interesting to see whether the difference between the experiment and Paris.exC suggested for T_{21} and T_{22} at around 110° really exists. The difference, if confirmed, may indicate the necessity to improve the tensor part of the Paris NN potential.

VI. SUMMARY AND CONCLUSION

The vector and tensor analyzing powers of the $p+d$ scattering have been measured precisely at $E_p = 2.5$ MeV ($E_d = 5$ MeV), where the Coulomb force has been treated nearly correctly in a $p+d$ Faddeev calculation. The measurements have also been made at $E_p = 2, 3,$ and 4 MeV, and at $E_d = 6$ MeV. The high accuracies of the present data have enabled the unambiguous comparison between the experiment and the calculations below and slightly above the deuteron breakup threshold.

The present data on the analyzing powers and our previous data on the differential cross section in the same energy range [9] have been compared with the Faddeev calculations based on a separable-form NN potential with the nearly correct treatment of the Coulomb force (PEST.exC) and those based on the original or the LS -modified Paris NN potentials with the approximate treatment of the Coulomb force (Paris.apC and modLS.apC). Although a Faddeev calculation based on a realistic NN potential, e.g., the Paris potential, with the correct treatment of the Coulomb force (Paris.exC) has not been performed yet, we can infer to some extent its possible prediction from the combinations of the above calculations.

A discrepancy between the experiment and the inferred

Paris.exC is considered to exist in the $p+d$ differential cross section around 115° at $E_p = 2.5$ MeV. The discrepancy seems to be energy dependent as has been suggested already in our previous work [9]. The large disagreement in A_y around its maximum near 115° between the experiment and the calculation has been well known for $N+d$ scattering below 20 MeV. In the present low-energy range the disagreement is also confirmed to exist. A similarly large disagreement of slightly different character is recognized for iT_{11} at $E_d = 5$ and 6 MeV. Moreover, it is pointed out in the present work that the tensor analyzing powers T_{21} and T_{22} around $\theta_{c.m.} = 115^\circ$ are expected to disagree with the Paris.exC. Hence the disagreements seem to exist in all the scalar, the vector, and the tensor observables of the $p+d$ scattering between the experiment and the calculation based on the realistic NN potential with the exact treatment of the Coulomb force (Paris.exC).

It should be investigated whether the disagreements can be reduced by improving the NN potential or by introducing some reaction mechanisms neglected so far in the calculation. It is also interesting to see whether the scalar, vector, and tensor parts of the NN potential has to be improved individually or if there is one missing term responsible for all the kinds of discrepancies. As an example in the former viewpoint, the modification in the LS potential by Takemiya [7] has been successful in reducing the discrepancies in the vector analyzing powers. However, the discrepancies in the cross section and the tensor analyzing powers remain unchanged. As for the latter trial, it has been reported that the inclusion of a 2π -exchange $3N$ force even enlarges the discrepancy in A_y [3], though the $3N$ force of the same kind has been effective to reproduce the $3N$ binding energy [23]. Further theoretical attempts are desired together with the improved treatment of the Coulomb force below and above the deuteron breakup threshold.

To systematically investigate the energy dependence of the discrepancies in the tensor analyzing powers, precise experiments on the $\vec{d}+p$ scattering at higher energies are also necessary.

ACKNOWLEDGMENTS

The authors wish to thank Professor T. Takemiya for his intimate communications and his permission for the use of his computer code, Professor Y. Koike and Professor S. Oryu for their valuable discussions, and Y. Koga and T. Maeda for preparing experimental instruments. This work was supported in part by Japan Ministry for Education, Science and Culture under Grant-in-Aid No. 0352023.

-
- [1] T. Takemiya, Prog. Theor. Phys. **74**, 301 (1985).
 [2] H. Witala, W. Glöckle, and T. Cornelius, Few Body Syst. **3**, 123 (1988); Nucl. Phys. **A491**, 157 (1989).
 [3] H. Witala, D. Hüber, and W. Glöckle, Phys. Rev. C **49**, R14 (1994).
 [4] G. H. Berthold, A. Stadler, and H. Zankel, Phys. Rev. C **41**, 1365 (1990).
 [5] Y. Koike and J. Haidenbauer, in Proceedings of 11th Confer-

- ence on Few-Body Problems in Physics, Sendai, 1986 [Nucl. Phys. **A463**, 365c (1987)].
 [6] H. Witala and W. Glöckle, Nucl. Phys. **A528**, 48 (1991); H. Witala, W. Glöckle, and H. Kamada, Phys. Rev. C **43**, 1619 (1991).
 [7] T. Takemiya, Prog. Theor. Phys. **86**, 975 (1991).
 [8] S. Oryu and H. Yamada, Phys. Rev. C **50**, 2337 (1994).
 [9] K. Sagara, H. Oguri, S. Shimizu, K. Maeda, H. Nakamura, T.

- Nakashima, and S. Morinobu, *Phys. Rev. C* **50**, 576 (1994).
- [10] T. Takemiya (private communication).
- [11] P. Doleschall, W. Grüebler, V. König, P. A. Schmelzbach, F. Sperisen, and B. Jenny, *Nucl. Phys.* **A380**, 72 (1982).
- [12] J. B. Marrion and B. A. Zimmermen, *Nucl. Instrum. Methods* **51**, 93 (1967).
- [13] R. A. Arndt, D. D. Long, and L. D. Roper, *Nucl. Phys.* **A209**, 429 (1973); R. A. Arndt, L. D. Roper, and R. L. Shotwell, *Phys. Rev. C* **3**, 2100 (1971).
- [14] D. C. Dodder, G. M. Hale, N. Jarmie, J. H. Jett, P. W. Keaton, Jr., R. A. Nisley, and K. Witte, *Phys. Rev. C* **15**, 518 (1977).
- [15] S. Tharraketa, W. Arnold, H. Baumgart, J. Günzl, A. Hofmann, E. Huttel, N. Kniest, and G. Clausnitzer, *J. Phys. Soc. Jpn. B* **55**, 880c (1986).
- [16] G. R. Plattner and A. D. Bacher, *Phys. Lett.* **36B**, 211 (1971).
- [17] K. Sagara, K. Maeda, H. Nakamura, M. Izumi, T. Yamaoka, Y. Nishida, M. Nakashima, and T. Nakashima, *Nucl. Instrum. Methods* **A270**, 444 (1988).
- [18] B. A. Jacobsohn and R. M. Ryndin, *Nucl. Phys.* **A24**, 505 (1961).
- [19] W. Grüebler, P. A. Schmelzbach, and V. König, *Phys. Rev. C* **22**, 2243 (1980).
- [20] G. G. Ohlsen, J. L. Mackibben, R. R. Stevens, Jr., and G. P. Lawrence, *Nucl. Instrum. Methods* **73**, 45 (1969).
- [21] R. E. White, W. Grüebler, B. Jenny, V. König, P. A. Schmelzbach, and H. R. Burgi, *Nucl. Phys.* **A321**, 1 (1979).
- [22] L. D. Knutson, L. O. Lamm, and J. E. McAninch, *Phys. Rev. Lett.* **71**, 3762 (1993).
- [23] T. Sasakawa, S. Ishikawa, Y. Wu, and T-Y. Saito, *Phys. Rev. Lett.* **68**, 3503 (1992).